npj | Quantum Information

www.nature.com/npjqi

ARTICLE OPEN

Check for updates

# Beyond the standard quantum limit for parametric amplification of broadband signals

M. Renger[1,2]✉, S. Pogorzalek[1,2], Q. Chen[1,2], Y. Nojiri[1,2], K. Inomata[3,4], Y. Nakamura[3,5], M. Partanen[1], A. Marx[1], R. Gross[1,2,6], F. Deppe[1,2,6] and K. G. Fedorov[1,2]✉

The low-noise amplification of weak microwave signals is crucial for countless protocols in quantum information processing. Quantum mechanics sets an ultimate lower limit of half a photon to the added input noise for phase-preserving amplification of narrowband signals, also known as the standard quantum limit (SQL). This limit, which is equivalent to a maximum quantum efficiency of 0.5, can be overcome by employing nondegenerate parametric amplification of broadband signals. We show that, in principle, a maximum quantum efficiency of unity can be reached. Experimentally, we find a quantum efficiency of 0.69 ± 0.02, well beyond the SQL, by employing a flux-driven Josephson parametric amplifier and broadband thermal signals. We expect that our results allow for fundamental improvements in the detection of ultraweak microwave signals.

*npj Quantum Information* (2021)7:160 ; https://doi.org/10.1038/s41534-021-00495-y

## INTRODUCTION

In quantum technology, resolving low power quantum signals in a noisy environment is essential for an efficient readout of quantum states[1]. Linear phase-preserving amplifiers are a central tool to accomplish this task by simultaneously increasing the amplitude in both signal quadratures without altering the signal phase[2]. Due to the low energy of microwave photons, this amplification process is of particular relevance for the tomography of quantum microwave states[3]. State tomography is crucial for experimental protocols with quantum propagating microwaves such as entanglement generation[4–8], secure quantum remote state preparation[9], quantum teleportation[10–12], quantum illumination[13], or quantum state transfer[14]. Furthermore, a conventional dispersive readout of superconducting qubits[15–22] relies on the amplification of microwave signals which carry information about the qubit and consist only of a few photons[23]. This approach has proven to be extremely successful and has led to the realization of important milestones in superconducting quantum information processing[24,25]. However, fundamental laws of quantum physics imply that any phase-preserving amplifier needs to add at least half a noise photon in the high-gain limit [26]. This bound is known as the standard quantum limit (SQL) and results from the bosonic commutation relations of input and output fields constituting the original and amplified signals, respectively. Quantum-limited amplification of quantum microwave states has been achieved with superconducting Josephson parametric amplifiers (JPAs)[27–29], but also by employing Josephson traveling-wave parametric amplifiers (JTWPAs)[30]. With JTWPAs, a noise performance of 2.1 times the SQL has been reached[31]. Nevertheless, alternative ways to realize noiseless amplification are important for a large variety of quantum applications which rely on the efficient detection of signal amplitudes such as the parity measurements in multi-qubit systems[32], quantum amplitude sensing[33], detection of dark matter axions[34], or the detection of the cosmic microwave background[35], among others.

In this work, we investigate the nondegenerate parametric amplification of broadband microwave signals and derive conditions under which noiseless amplification is possible. This broadband nondegenerate regime is realized by employing a flux-driven JPA and is complimentary to the conventional phase-preserving nondegenerate (narrowband and quantum-limited) or phase-sensitive degenerate (narrowband and potentially noiseless) regimes[36–38]. In the current context, the terms 'narrowband' and 'broadband' relate to the bandwidth of input signals and not to the bandwidth of the JPA itself. It is important to emphasize that, in contrast to the degenerate regime, signal and idler are separate frequency modes here. Their phases can be, in principle, either correlated or uncorrelated, which leads to the phase-dependent or phase-independent amplification regimes, respectively. One could also note that the nondegenerate amplifier allows to realize a two-mode squeezing operation between the input signal and input idler modes[39,40]. Here, we experimentally demonstrate a JPA for the phase-independent linear amplification of broadband signals with performance beyond the SQL.

## RESULTS

### Quantum limits on quantum efficiency

An ideal linear amplifier increases the signal photon number $n_s$ by the power gain factor $G_n^2$. The fluctuations in the output signal consist of the amplified vacuum fluctuations of the input signal and the noise photons $n_f$, added by the amplifier, where $n_f$ is referred to the amplifier input. We use the quantum efficiency $\eta$ to characterize the noise performance of our amplifiers[41]. The quantum efficiency is defined as the ratio between vacuum fluctuations in the input signal and fluctuations in the output signal. Thus, $\eta$ can be expressed as

$$\eta = \frac{1}{1 + 2n_f}. \quad (1)$$

[1]Walther-Meißner-Institut, Bayerische Akademie der Wissenschaften, 85748 Garching, Germany. [2]Physik-Department, Technische Universität München, 85748 Garching, Germany. [3]RIKEN Center for Emergent Matter Science (CEMS), Wako, Saitama 351-0198, Japan. [4]National Institute of Advanced Industrial Science and Technology, 1-1-1 Umezono, Tsukuba, Ibaraki 305-8563, Japan. [5]Research Center for Advanced Science and Technology (RCAST), The University of Tokyo, Meguro-ku, Tokyo 153-8904, Japan. [6]Munich Center for Quantum Science and Technology (MCQST), Schellingstr. 4, 80799 Munich, Germany. ✉email: michael.renger@wmi.badw.de; kirill.fedorov@wmi.badw.de

Parametrically driving the JPA results in amplification of the incoming signal and creation of an additional phase-conjugated idler mode. This idler mode consists of, at least, vacuum fluctuations, implying that it carries $n_\mathrm{i} \geq 1/2$ photons. As a result of the narrowband parametric signal amplification, the idler adds[42]

$$n_\mathrm{f} = n_\mathrm{i}\frac{G_\mathrm{n}-1}{G_\mathrm{n}} \geq \frac{1}{2}\left(1-\frac{1}{G_\mathrm{n}}\right) \tag{2}$$

noise photons to the signal, referred to the amplifier input, as schematically depicted in Fig. 1a. Equation (2) implies that $\eta$ is bounded by

$$\eta \leq \frac{G_\mathrm{n}}{2G_\mathrm{n}-1}, \tag{3}$$

reaching 1/2 in the high-gain limit, $G_\mathrm{n} \gg 1$. Figure 1b illustrates the amplification process for broadband signals, where the input signal bandwidth is large enough to cover both the signal and idler modes of the parametric amplifier. As a result, the idler mode does not add any noise but contributes to the amplified output signal. Thus, we expect that a quantum efficiency of $\eta = 1$ can be reached in this case.

### Nondegenerate Josephson parametric amplifier

Parametric amplification can be realized by driving a nonlinear electromagnetic resonator with a strong coherent field (pump) at $\omega_\mathrm{p} = 2\omega_0$, where $\omega_0$ is the resonance frequency[37,42]. In the resulting three-wave mixing process, a pump photon splits into a signal photon at frequency $\omega_\mathrm{s} = \omega_\mathrm{p}/2 + \Delta$ and a corresponding idler photon at $\omega_\mathrm{i} = \omega_\mathrm{p}/2 - \Delta$. Here, $\Delta$ denotes the detuning of the signal reconstruction frequency $\omega_\mathrm{s}$ from $\omega_0$. In the nondegenerate regime, we have $\Delta \neq 0$, leading to spectrally separated signal and idler modes[43]. This parametric down-conversion process results in a Lorentzian spectral gain function, which is depicted by the purple solid line in Fig. 1a, bottom. The input signal as well as the amplified output signal is detected within the measurement bandwidth $2B$ around $\omega_\mathrm{s}$. For a narrowband state, the idler necessarily adds broadband noise to the signal, leading to broadening of the output variances (see Fig. 1a, top). In contrast, if the signal bandwidth $b_\mathrm{s}$ is large enough to cover the idler input modes, as shown in Fig. 1b, the amplified output signal consists of contributions from both the signal and idler modes. In this case, the idler no longer serves as a noise port but rather as an additional signal port and the part of the input signal at the idler frequency is mixed into the measurement bandwidth. In the case where the input signal phase and the input idler phase are uncorrelated, we obtain a total broadband gain (see Supplemental Material).

$$G_\mathrm{b} = 2G_\mathrm{n} - 1. \tag{4}$$

### Standard quantum limit for multimode input signals

The SQL fundamentally results from the fact that the amplifier input and output signals have to fulfill the bosonic commutation relations. We assume that the JPA output $\hat{c}(\omega)$ results from a linear combination of amplified incoming signals $\hat{a}(\tilde{\omega})$ and phase-conjugated idler signals $\hat{a}^\dagger(\tilde{\omega}_\mathrm{i})$ as well as from an additive noise mode $\hat{f}(\omega)$[26]

$$\hat{c}(\omega) = \int_{\mathcal{I}} d\tilde{\omega}\left[M(\omega,\tilde{\omega})\hat{a}(\tilde{\omega}) + L(\omega,\tilde{\omega})\hat{a}^\dagger(\tilde{\omega})\right] + \hat{f}(\omega), \tag{5}$$

where the integral is taken over all input modes $\mathcal{I}$. Frequencies $\tilde{\omega}$ denote input modes, whereas output modes are described by $\omega$. We assume that the input signal is centered around the frequency $\omega_\mathrm{s}$ and has a single-side bandwidth $b_\mathrm{s}$ (total bandwidth $2b_\mathrm{s}$). The signal amplitude gain $M(\omega,\tilde{\omega})$ and the idler amplitude gain $L(\omega,\tilde{\omega})$ satisfy $M(\omega,\tilde{\omega}) = M(\tilde{\omega})\delta(\omega-\tilde{\omega})$ and $L(\omega,\tilde{\omega}) = L(\tilde{\omega}_\mathrm{i})\delta(\omega-\tilde{\omega}_\mathrm{i})$, respectively, where $\tilde{\omega}_\mathrm{i} = 2\omega_0 - \tilde{\omega}$. Furthermore, $|M(\omega)|^2 = G_\mathrm{n}(\omega)$ and $|L(\omega_\mathrm{i})|^2 = G_\mathrm{n}(\omega) - 1$, where $G_\mathrm{n}(\omega)$ is the power gain. The strength of the additive noise is described with the noise power spectral density $S_\mathrm{f}(\omega)$ of the bosonic mode $\hat{f}(\omega)$, corresponding to the number of noise photons per mode. We evaluate the integral in Eq. (5) and calculate the commutator $[\hat{c}(\omega), \hat{c}^\dagger(\omega')]$. Next, we calculate the spectral autocorrelation function of the fluctuations. This allows us to use the bosonic continuum commutation relations and the Heisenberg uncertainty principle to show that

$$\begin{aligned}\int_{\omega_\mathrm{s}-b_\mathrm{s}}^{\omega_\mathrm{s}+b_\mathrm{s}} S_\mathrm{f}(\omega)d\omega &\equiv 2b_\mathrm{s}n_\mathrm{f} \geq 2b_\mathrm{s}n_\mathrm{ql} \\ &= \tfrac{1}{2}\int_{\omega_\mathrm{s}-b_\mathrm{s}}^{\omega_\mathrm{s}+b_\mathrm{s}}\left[1 - \mathbb{1}_\mathrm{i}(\omega) + \tfrac{1}{G_\mathrm{n}(\omega)}\left(\mathbb{1}_\mathrm{i}(\omega)-1\right)\right]d\omega,\end{aligned} \tag{6}$$

where $n_\mathrm{ql}$ is the quantum limit for the number of additive noise photons (see Supplemental Material). We define

$$\mathbb{1}_\mathrm{i}(\omega) = \Theta(\omega - 2\omega_0 + \omega_\mathrm{s} + b_\mathrm{s}) - \Theta(\omega - 2\omega_0 + \omega_\mathrm{s} - b_\mathrm{s}), \tag{7}$$

where $\Theta$ is the Heaviside step function. In Eq. (6), the range of integration over $\omega$ is limited by $b_\mathrm{s}$, if $b_\mathrm{s} < B$, otherwise it is set by $B$. We observe that there are two threshold values of the bandwidth: $b_1 = 2\Delta - B$ and $b_2 = 2\Delta + B$. For $b_\mathrm{s} \leq b_1$, Eq. (6) reproduces the SQL, whereas for $b_1 \leq b_\mathrm{s} \leq b_2$, the input signal starts to overlap with idler modes and the lower bound for the additive noise decreases. In the broadband case $b_\mathrm{s} \geq b_2$, the signal covers all idler modes and Eq. (6) reduces to $n_\mathrm{f} \geq 0$, implying that there is no fundamental lower limit for the added noise.

### Experimental setup

Our experimental setup is schematically shown in Fig. 1c and consists of a flux-driven JPA serially connected to a cryogenic high-electron-mobility transistor (HEMT) amplifier with a gain of $G_\mathrm{H} = 41$ dB. The JPA is operated in the nondegenerate regime, which is realized by detuning the signal frequency $\omega_\mathrm{s}$ by $\Delta/2\pi = 300$ kHz from half the pump frequency $\omega_\mathrm{p}/2 = \omega_0$. A circulator at the JPA input separates the resonator input and output fields. The moments of the output signal are reconstructed with a bandwidth $B/2\pi = 200$ kHz using the reference-state reconstruction method at the reconstruction point indicated by the red circle in Fig. 1c[7,44]. The experiment is performed with two distinct JPAs, labelled JPA 1 and JPA 2, which are operated at different flux spots to check for reproducibility of our results. For JPA 1 (JPA 2), we reconstruct the signal at $\omega_\mathrm{s}/2\pi = 5.500$ GHz (5.435 GHz). A continuous coherent tone can be applied via a microwave input line and a heatable 30 dB attenuator allows us to generate thermal states as broadband input signals.

### Bandwidth dependence of the limits on quantum efficiency

We solve Eq. (6) for the Lorentzian JPA gain function $G_\mathrm{n}(\omega) = 1 + G_0 b_\mathrm{J}^2/(b_\mathrm{J}^2 + (\omega-\omega_0)^2)$, where $G_0$ denotes the maximal JPA gain and $b_\mathrm{J}$ is the half width at half maximum JPA bandwidth[43]. Then, assuming $G_0 \gg 1$, the quantum limit $n_\mathrm{ql}$ for the number of additive noise photons is given by

$$n_\mathrm{ql} = \frac{1}{4\beta}\begin{cases}\arctan\left(\frac{2\beta}{1+\delta^2-\beta^2}\right) & B \leq b_\mathrm{s} \leq b_1, \\ \arctan\left(\frac{2(\delta+\beta-\beta_\mathrm{s})}{1+\beta\beta_\mathrm{s}+\delta(\beta_\mathrm{s}-\beta)-\delta^2}\right) & b_1 \leq b_\mathrm{s} \leq b_2, \\ 0 & b_\mathrm{s} \geq b_2,\end{cases} \tag{8}$$

with $\beta = B/\tau$, $\beta_\mathrm{s} = b_\mathrm{s}/\tau$, and $\delta = \Delta/\tau$, where $\tau \equiv b_\mathrm{J}\sqrt{G_0}$ denotes the gain-bandwidth product[36] (see Supplemental Material). The corresponding limit $\eta_\mathrm{ql}$ of the quantum efficiency $\eta$ can be calculated with Eq. (1). The case $b_\mathrm{s} \leq B$ is not considered in Eq. (8) as it is only of technical relevance since we can always achieve $b_\mathrm{s} = B$ by adopting $B$. A discussion of this case is included in the supplement (see Supplemental Material). The solution Eq. (8) allows us to distinguish quantitatively between broadband and narrowband regimes and is plotted for $\tau/2\pi = 15$ MHz in Fig. 2a for varying $\Delta$ with $B/2\pi = 30$ kHz and in Fig. 2b for varying $B$ with $\Delta/2\pi = 37.5$ kHz. According to Eq. (8), we obtain $\eta_\mathrm{ql} = 1/2$ for

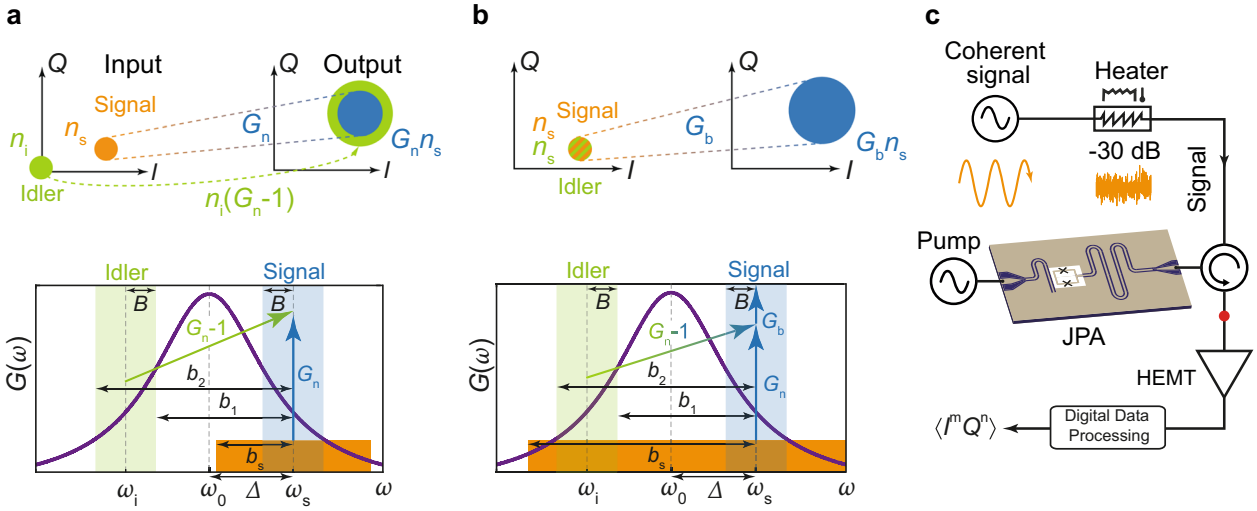


**Fig. 1 Phase space representation of nondegenerate parametric amplification and experimental setup. a** Top: Phase space transformation for the amplification of narrowband input signals. Colored circles depict the respective variances of the input signal (orange), output signal (blue), and idler mode (green). Bottom: Spectrum of parametric amplification of narrowband signals with bandwidth $b_s$. The purple solid line shows a Lorentzian gain function. Blue-shaded and green-shaded regions represent measurement bands with full bandwidth $2B$ around the signal and idler modes, respectively. For input signals with $b_s \leq b_1$, the idler adds at least vacuum fluctuations to the output. **b** Top: Phase space transformation for amplification of broadband input signals. The idler does no longer act as a noise port and the signal is amplified with gain $G_b = 2G_n - 1$. Bottom: Spectrum of parametric amplification process for broadband signals. If $b_s \geq b_2$, each mode in the signal bandwidth corresponds to a correlated input mode on the idler side, resulting in amplification with the total gain $G_b$ and the absence of the SQL. **c** Illustration of the experimental setup. The amplification chain consists of a nondegenerate Josephson parametric amplifier (JPA) and a cryogenic HEMT amplifier. Narrowband coherent states can be applied via a microwave source and a heatable attenuator enables the generation of broadband thermal states. The red dot labels the signal reconstruction point.

coherent input signals, approximately reproducing Eq. (3), whereas we expect $\eta_{ql} = 1$ for broadband signals.

### Experimental determination of the quantum efficiency

We experimentally extract the quantum efficiency by measuring the total noise photon number of the amplification chain. To achieve this goal, we vary the temperature of the heatable 30 dB attenuator from 40 mK to 600 mK and perform Planck spectroscopy of the amplification chain[45]. As a result, we detect the photon number $n_b$ at the reconstruction point for varying broadband gain $G_b$ and show the result of this measurement in Fig. 3a for JPA 2. For each value of $G_b$, the experimentally determined outcomes for $n_b$ (dots) are fitted with corresponding Planck distributions (cyan solid lines) and the respective noise photon number is extracted from the offset. The quantum efficiency for narrowband signals is determined in a similar experiment by amplifying a coherent input tone with varying input photon number $n_{in}$ for different JPA gains $G_n$. For each value of $G_n$, the amplifier response $n_n$ at the reconstruction point is linearly fitted, which allows us to extract the noise photons from the respective offset. This procedure also proves that the JPA acts as a linear amplifier here. Figure 3b shows a logarithmic plot of the experimental results (dots) for JPA 2 as well as the respective linear fits (orange lines). The dependence of the broadband gain $G_b$ on $G_n$ is depicted in Fig. 3c. The results are in agreement with Eq. (4).

In Fig. 4a, we plot the measured quantum efficiencies for JPA 1 for the amplification of thermal states (cyan dots) and coherent states (purple dots), respectively. The red dashed line depicts the SQL determined by Eq. (3). Figure 4b shows the result for the same experiment with JPA 2 instead of JPA 1. For both JPAs, we find a gain region where we clearly exceed the SQL for the amplification of broadband states.

### Experimental limitations on quantum efficiency

Importantly, Fig. 4b shows that we can achieve a maximal quantum efficiency $\eta = 0.69 \pm 0.02$ with our setup, which substantially exceeds the SQL. This value is comparable to quantum efficiencies reached with degenerate phase-sensitive JPAs[36,46] and is notably higher than the quantum efficiency of 0.32 reached with the phase-preserving JTWPA in ref. [31]. The deviation from the theoretically achievable quantum efficiency of unity can be explained by noise in the pump signal, as discussed below. Furthermore, we observe that the experimentally determined dependence of quantum efficiency on the gain in Fig. 4 reaches a maximum and decreases for higher gains for the narrowband and broadband case. For low JPA gains, the noise photons $n_H = 11.3$, which are added by the HEMT, limit the quantum efficiency. This contribution becomes irrelevant in the high-gain limit, since its influence decreases with $1/G$, where $G = G_n$ ($G = G_b$) for narrowband (broadband) amplification. Since the parametric gain depends on the pump power, fluctuations in the pump photon number imply additional noise in the signal mode[47]. We describe the noisy pump signal in the frame rotating at a pump frequency $\omega_p$ by

$$\hat{A}(t) = (a_0 + \hat{f}_p(t))e^{-i\omega_p t}, \tag{9}$$

where $a_0$ denotes the amplitude of the coherent pump signal and the operator $\hat{f}_p(t)$ represents thermal noise. We use the Wiener–Khinchin theorem to calculate the variance of the corresponding power fluctuations (see Supplemental Material)[48]. The experimentally determined dependence of the parametric gain on the pump power can be fitted by an exponential function (see Supplemental Material). Thus, the gain-dependent JPA noise $n_J(G)$ can be approximated by

$$n_J(G) = n_J'(G-1)^{\epsilon}, \tag{10}$$

where $\epsilon$ depends on JPA parameters and $n_J'$ is a constant prefactor (see Supplemental Material). We use Eq. (10) to fit the measured quantum efficiencies in Fig. 4a, b and treat $n_J'$ and $\epsilon$ as fitting parameters. In Fig. 4a, the last data point for broadband amplification is not considered for the fit, as JPA 1 starts entering a nonlinear compression regime. The fit is depicted by the solid lines in Fig. 4a, b for both JPAs and successfully reproduces the maximum as well as the behavior for low gain values.

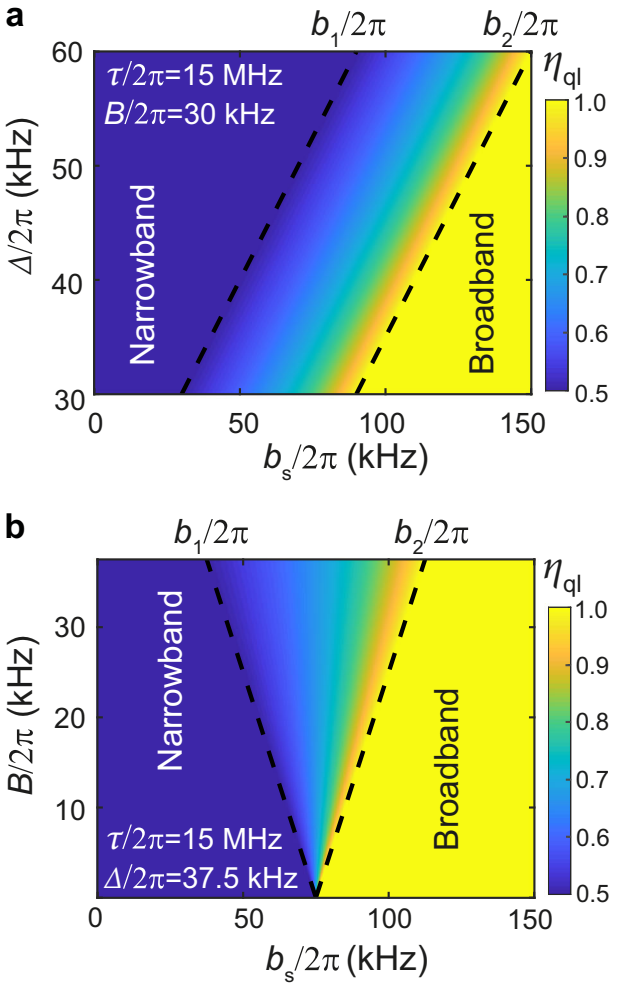


**Fig. 2 Theoretical limits on quantum efficiency.** Limit $\eta_{ql}$ of the quantum efficiency $\eta$ as a function of the signal bandwidth $b_s$ for **a** varying detuning $\Delta$ at a fixed measurement bandwidth $B/2\pi = 30$ kHz and **b** for varying measurement bandwidth $B$ at a fixed detuning $\Delta/2\pi = 37.5$ kHz, according to Eq. (8). For $b_s \geq b_2$, amplification with $\eta = 1$ is possible. The case $b_s \leq B$ is only of technical interest and is discussed in the supplement (see Supplemental Material).

## DISCUSSION

In conclusion, we have investigated a nondegenerate linear parametric amplification of broadband signals and have derived a quantitative criterion for an input signal bandwidth under which a quantum efficiency of $\eta = 1$ can be achieved. We have used a superconducting flux-driven JPA to experimentally determine the quantum efficiencies for amplification of broadband thermal states and demonstrated $\eta = 0.69 \pm 0.02$ which significantly exceeds the SQL $\eta_{ql} = 0.5$. Thus, we have verified that for the parametric amplification of broadband input states, an idler mode may also carry signal information and does not add extra noise to the output. However, the SQL violation in our experiment comes not from the phase interference but rather from the fact that average amplitudes for both the signal and idler modes encode the original signal information (see Supplemental Material). Since it is difficult to define a phase for a general broadband signal, which results from the technical difficulty to stabilize the relative phase of signal and idler in case of non-commensurable frequencies, encoding information in the photon number is a more natural choice. The absence of the SQL is furthermore reflected by the fact that the idler mode does not simply lead to a constant power offset, but alters the amplifier gain. This experimental observation is in stark contrast with the conventional phase-sensitive amplification regime, where the SQL violation relies on the phase interference. In our case, the latter is impossible due to the absence of any phase correlations in broadband thermal signals used for amplification. However, although a relative phase between signal and idler does not have an impact on the quantum limit for the noise, the amplifier output itself can depend on such a phase relationship. Furthermore, we have shown that the gain dependence of $\eta$ can be explained by the photon number fluctuations in the pump tone. One can exploit quantum efficiencies above the SQL $\eta > 0.5$ in experiments where ultra low-noise amplification is a key prerequisite. For instance, it can be used for high-efficiency parity detection of entangled superconducting qubits via readout of dispersively coupled resonators[20]. Assuming that these resonators are probed at the respective signal and idler frequencies of a readout JPA, one can amplify the combined resonator response with quantum efficiency beyond the SQL. Another useful application could be a direct broadband dispersive qubit readout with weak thermal states generated artificially or naturally occurring due to finite temperatures of the cryogenic environment[49].

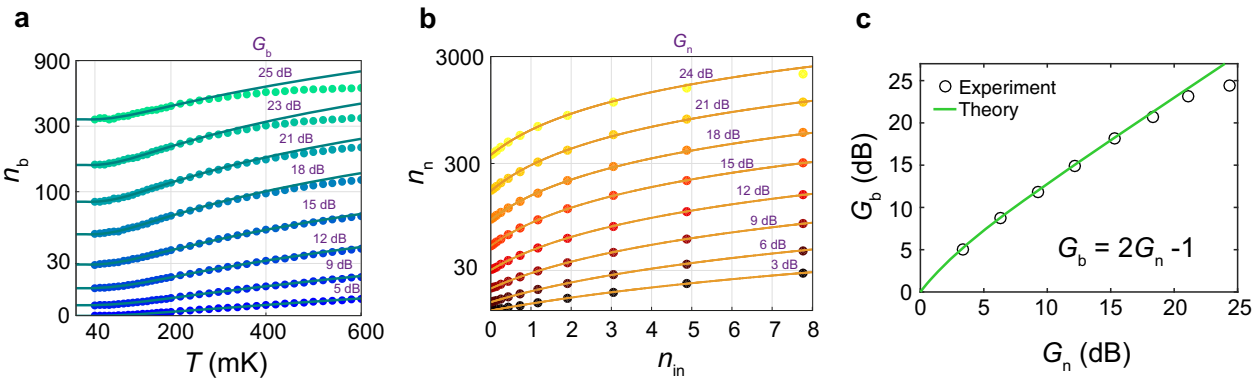


**Fig. 3 Experimental determination of quantum efficiency. a** Planck spectroscopy for varying broadband gain $G_b$. The average photon number $n_b$ of the amplified signal (dots) is indicated at the reconstruction point. The lines are fits to the corresponding Planck distributions. **b** Average photon number $n_n$ of the amplified signal (dots) at the reconstruction point for the amplification of a continuous coherent signal for different values of the narrowband gain $G_n$. The average photon number of the input signal is labeled with $n_{in}$. From the offsets of the linear fits (lines), we can calculate the number of added noise photons. **c** Experimentally determined broadband gain $G_b$ vs. narrowband gain $G_n$ of the JPA.

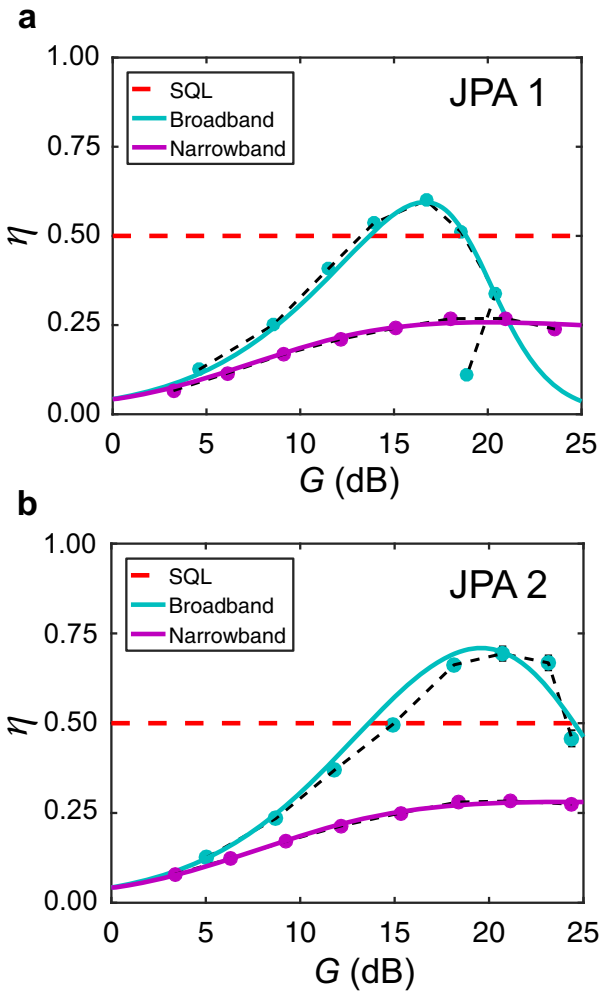


**Fig. 4 Quantum efficiency for nondegenerate broadband and narrowband amplification.** Experimental quantum efficiency of the flux-driven JPAs for broadband (cyan dots) and narrowband (purple dots) input signals. Panel **a** shows the data for JPA 1 and panel **b** the data for JPA 2. The red dashed line represents the SQL. The gain dependence of the quantum efficiencies for the narrowband and broadband cases is fitted using Eq. (10).

## METHODS

### Extracting the quantum efficiency for broadband signals

To measure the noise added by the amplification of broadband input signals, we vary the temperature $T_a$ of the heatable 30 dB attenuator from 40 mK to 600 mK using a PID control architecture. We detect the quadrature moments $\langle I^m Q^n\rangle$ with $m,n\in\mathbb{N}_0$, $m+n\le 4$ from the digitized and filtered output signal. The detected power $P(T_a)$ is determined by the sum $\langle I^2\rangle+\langle Q^2\rangle$ of the second order moments and follows a Planck curve[45]

$$\begin{aligned}P(T_a) &= \tfrac{\langle I^2\rangle+\langle Q^2\rangle}{R}\\ &= \tfrac{\kappa G_b \tilde{G}}{R}\left[\tfrac{1}{2}\coth\left(\tfrac{\hbar\omega_s}{2k_B T_a}\right)+n_{f,b}\right],\end{aligned} \tag{11}$$

where $n_{f,b}$ is the total noise added by the amplification chain referred to the input, $R=50\,\Omega$ is the line impedance, $G_b$ is the broadband JPA gain, $\tilde{G}$ is the gain of the HEMT and the remaining amplification chain and $\kappa$ denotes the photon-number-conversion factor (PNCF). The gain dependence of $n_{f,b}$ can be determined by repeating the temperature sweep for varying values of $G_b$ and fitting a Planck curve to each of the results. To be able to experimentally control $G_b$, we use a vector network analyzer to measure the pump power dependence of the narrowband parametric gain $G_n$. We then expect $G_b=G_n+3$ dB and measure Planck curves for expected $G_b$ ranging from 6 dB to 27 dB in steps of 3 dB and fit Eq. (11) to each experimental outcome. Since we measure with a two-pulsed scheme, where the JPA pump signal is only switched on during the second pulse, $G_b$ can be extracted directly from the measurement by calculating the ratio of the prefactors $G_b\tilde{G}$ of the Planck curves corresponding to the second pulse and first pulse. We calculate the broadband quantum efficiencies $\eta_b=1/(1+2n_{f,b})$ from the fit parameters. The error bars for the quantum efficiency are determined from the fit error $\Delta n_{f,b}$ by error propagation.

### Extracting the quantum efficiency for narrowband signals

To calibrate the photon number in a coherent input signal, we switch the JPA pump off and tune the JPA resonance frequency out of the measurement bandwidth such that the JPA does not have any impact on the calibration procedure. We then perform Planck spectroscopy to determine the PNCF for the signal reconstruction point[45]. Following that, we vary the power $P_{coh}$ of the coherent input signal and determine the photon number $n_{coh}$ at the reconstruction point using the reference-state reconstruction method for each value of $P_{coh}$ (see Supplemental Material). This data can be linearly fitted according to

$$n_{coh}(P_{coh}) = k_1 P_{coh} + k_2, \tag{12}$$

where $k_1$ and $k_2$ are fitting parameters. To measure the additive noise number, we tune the JPA into resonance and measure in the two-pulsed scheme. We vary the coherent input photon number $n_{in}$ and measure the output photon number $n_{out}$ for the case in which the JPA pump is switched off (first pulse). We repeat the measurement and detect the signal power $n_{JPA}$ when the JPA pump is switched on. Both results are fitted linearly according to

$$n_{out} = k_3 n_{in} + k_4, \tag{13}$$

$$n_{JPA} = k_5 n_{in} + k_6 \tag{14}$$

with fitting constants $k_3$, $k_4$, $k_5$, $k_6$. From this, we extract the narrowband gain $G_n=k_5/k_3$ and the total number of added noise photons $n_{f,n}=k_6/G_n$, referred to the input which allows us to calculate the narrowband quantum efficiency $\eta_n$. The error bars for $\eta_n$ are determined from the fit by error propagation.

### Fitting the measured quantum efficiencies

The total additive noise $n_f$, referred to the input of the amplification chain, can be related to the JPA noise $n_J$ and the HEMT noise $n_H$ with the Friis equation[50]

$$n_f = n_J + \frac{n_H}{G}, \tag{15}$$

where $G$ denotes the JPA gain (either narrowband or broadband). Thus, we can express the quantum efficiency $\eta$ as

$$\eta = \frac{G}{G+2Gn_J+2n_H}. \tag{16}$$

The JPA noise $n_J$ is dependent on $G$. For $G=1$, i.e., when the JPA is switched off, we expect $n_J=0$. We assume that the gain-dependent noise $n_{J,b}(G_b)$ for amplification of broadband signals mainly results from pump induced fluctuations and fit the measured quantum efficiencies for the broadband case using

$$\eta_b(G_b) = \frac{G_b}{G_b+2G_b n'_{J,b}(G_b-1)^{\epsilon_b}+2n_H}, \tag{17}$$

where we treat $n'_{J,b}$ and $\epsilon_b$ as fitting parameters and insert $n_H=11.3$ (see Supplemental Material). For the narrowband quantum efficiency $\eta_n$, we assume that the idler mode adds additional vacuum fluctuations to the signal. Thus, we assume for the noise photons

$$n_{J,n}(G_n) = \underbrace{n'_{J,n}(G_n-1)^{\epsilon_n}}_{\text{Pump-induced}} + \underbrace{\frac{1}{2}\left(1-\frac{1}{G_n}\right)}_{\text{SQL}}, \tag{18}$$

implying that we use

$$\eta_n(G_n) = \frac{G_n}{2G_n-1+2G_n n'_{J,n}(G_n-1)^{\epsilon_n}+2n_H} \tag{19}$$

as a fit function for this case, where we treat $n'_{J,n}$ and $\epsilon_n$ as fit parameters (see Supplemental Material).

## DATA AVAILABILITY

The data that support the findings of this study are available from the corresponding authors upon reasonable request.

Received: 27 May 2021; Accepted: 28 September 2021;
Published online: 08 November 2021

## REFERENCES

1. Clerk, A. A., Devoret, M. H., Girvin, S. M., Marquardt, F. & Schoelkopf, R. J. Introduction to quantum noise, measurement, and amplification. *Rev. Mod. Phys.* **82**, 1155–1208 (2010).
2. Caves, C. M., Combes, J., Jiang, Z. & Pandey, S. Quantum limits on phase-preserving linear amplifiers. *Phys. Rev. A* **86**, 063802 (2012).
3. Mallet, F. et al. Quantum state tomography of an itinerant squeezed microwave field. *Phys. Rev. Lett.* **106**, 220502 (2011).
4. Menzel, E. P. et al. Path entanglement of continuous-variable quantum microwaves. *Phys. Rev. Lett.* **109**, 250502 (2012).
5. Flurin, E., Roch, N., Mallet, F., Devoret, M. H. & Huard, B. Generating entangled microwave radiation over two transmission lines. *Phys. Rev. Lett.* **109**, 183901 (2012).
6. Fedorov, K. G. et al. Displacement of propagating squeezed microwave states. *Phys. Rev. Lett.* **117**, 020502 (2016).
7. Fedorov, K. G. et al. Finite-time quantum entanglement in propagating squeezed microwaves. *Sci. Rep.* **8**, 6416 (2018).
8. Schneider, B. H. et al. Observation of broadband entanglement in microwave radiation from a single time-varying boundary condition. *Phys. Rev. Lett.* **124**, 140503 (2020).
9. Pogorzalek, S. et al. Secure quantum remote state preparation of squeezed microwave states. *Nat. Commun.* **10**, 2604 (2019).
10. Di Candia, R. et al. Quantum teleportation of propagating quantum microwaves. *EPJ Quantum Technol.* **2**, 25 (2015).
11. Braunstein, S. L. & Kimble, H. J. Teleportation of continuous quantum variables. *Phys. Rev. Lett.* **80**, 869–872 (1998).
12. Furusawa, A. et al. Unconditional quantum teleportation. *Science* **282**, 706–709 (1998).
13. Las Heras, U. et al. Quantum illumination reveals phase-shift inducing cloaking. *Sci. Rep.* **7**, 9333 (2017).
14. Bienfait, A. et al. Phonon-mediated quantum state transfer and remote qubit entanglement. *Science* **364**, 368–371 (2019).
15. Blais, A., Huang, R.-S., Wallraff, A., Girvin, S. M. & Schoelkopf, R. J. Cavity quantum electrodynamics for superconducting electrical circuits: an architecture for quantum computation. *Phys. Rev. A* **69**, 062320 (2004).
16. Goetz, J. et al. Second-order decoherence mechanisms of a transmon qubit probed with thermal microwave states. *Quantum Sci. Technol.* **2**, 025002 (2017).
17. Xie, E. et al. Compact 3d quantum memory. *Appl. Phys. Lett.* **112**, 202601 (2018).
18. Goetz, J. et al. Parity-engineered light-matter interaction. *Phys. Rev. Lett.* **121**, 060503 (2018).
19. Eddins, A. et al. High-efficiency measurement of an artificial atom embedded in a parametric amplifier. *Phys. Rev. X* **9**, 011004 (2019).
20. Ristè, D. et al. Deterministic entanglement of superconducting qubits by parity measurement and feedback. *Nature* **502**, 350–354 (2013).
21. Vepsäläinen, A. P. et al. Impact of ionizing radiation on superconducting qubit coherence. *Nature* **584**, 551–556 (2020).
22. Didier, N., Kamal, A., Oliver, W. D., Blais, A. & Clerk, A. A. Heisenberg-limited qubit read-out with two-mode squeezed light. *Phys. Rev. Lett.* **115**, 093604 (2015).
23. Blais, A., Girvin, S. M. & Oliver, W. D. Quantum information processing and quantum optics with circuit quantum electrodynamics. *Nat. Phys.* **16**, 247–256 (2020).
24. Kandala, A. et al. Hardware-efficient variational quantum eigensolver for small molecules and quantum magnets. *Nature* **549**, 242–246 (2017).
25. Arute, F. et al. Quantum supremacy using a programmable superconducting processor. *Nature* **574**, 505–510 (2019).
26. Caves, C. M. Quantum limits on noise in linear amplifiers. *Phys. Rev. D* **26**, 1817–1839 (1982).
27. Yamamoto, T. et al. Flux-driven josephson parametric amplifier. *Appl. Phys. Lett.* **93**, 042510 (2008).
28. Yurke, B. et al. Observation of parametric amplification and deamplification in a josephson parametric amplifier. *Phys. Rev. A* **39**, 2519–2533 (1989).
29. Mutus, J. Y. et al. Strong environmental coupling in a josephson parametric amplifier. *Appl. Phys. Lett.* **104**, 263513 (2014).
30. Grimsmo, A. L. & Blais, A. Squeezing and quantum state engineering with josephson travelling wave amplifiers. *npj Quantum Inf.* **3**, 20 (2017).
31. Macklin, C. et al. A near–quantum-limited josephson traveling-wave parametric amplifier. *Science* **350**, 307–310 (2015).
32. Takita, M. et al. Demonstration of weight-four parity measurements in the surface code architecture. *Phys. Rev. Lett.* **117**, 210505 (2016).
33. Joas, T., Waeber, A. M., Braunbeck, G. & Reinhard, F. Quantum sensing of weak radio-frequency signals by pulsed mollow absorption spectroscopy. *Nat. Commun.* **8**, 964 (2017).
34. Braine, T. et al. Extended search for the invisible axion with the axion dark matter experiment. *Phys. Rev. Lett.* **124**, 101303 (2020).
35. Braggio, C. et al. The measurement of a single-mode thermal field with a microwave cavity parametric amplifier. *New J. Phys.* **15**, 013044 (2013).
36. Zhong, L. et al. Squeezing with a flux-driven josephson parametric amplifier. *New J. Phys.* **15**, 125013 (2013).
37. Pogorzalek, S. et al. Hysteretic flux response and nondegenerate gain of flux-driven josephson parametric amplifiers. *Phys. Rev. Appl.* **8**, 024012 (2017).
38. Lecocq, F. et al. Microwave measurement beyond the quantum limit with a nonreciprocal amplifier. *Phys. Rev. Appl.* **13**, 044005 (2020).
39. Eichler, C. et al. Observation of two-mode squeezing in the microwave frequency domain. *Phys. Rev. Lett.* **107**, 113601 (2011).
40. Eichler, C., Salathe, Y., Mlynek, J., Schmidt, S. & Wallraff, A. Quantum-limited amplification and entanglement in coupled nonlinear resonators. *Phys. Rev. Lett.* **113**, 110502 (2014).
41. Boutin, S. et al. Effect of higher-order nonlinearities on amplification and squeezing in josephson parametric amplifiers. *Phys. Rev. Appl.* **8**, 054030 (2017).
42. Roy, A. & Devoret, M. Introduction to parametric amplification of quantum signals with josephson circuits. *C R Phys.* **17**, 740–755 (2016).
43. Yamamoto, T., Koshino, K. & Nakamura, Y. *Principles and Methods of Quantum Information Technologies* (Springer, 2016).
44. Eichler, C. et al. Experimental state tomography of itinerant single microwave photons. *Phys. Rev. Lett.* **106**, 220503 (2011).
45. Mariantoni, M. et al. Planck spectroscopy and quantum noise of microwave beam splitters. *Phys. Rev. Lett.* **105**, 133601 (2010).
46. Yurke, B. et al. Observation of 4.2-k equilibrium-noise squeezing via a josephson-parametric amplifier. *Phys. Rev. Lett.* **60**, 764–767 (1988).
47. Kylemark, P., Karlsson, M. & Andrekson, P. A. Gain and wavelength dependence of the noise-figure in fiber optical parametric amplification. *IEEE Photon. Technol. Lett.* **18**, 1255–1257 (2006).
48. Olsson, N. A. Lightwave systems with optical amplifiers. *J. Light. Technol.* **7**, 1071–1082 (1989).
49. Liu, G. et al. Noise reduction in qubit readout with a two-mode squeezed interferometer. Preprint at https://arxiv.org/abs/2007.15460 (2020).
50. Pozar, D. M. *Microwave Engineering* 4th edn (Wiley, 2012).

## ACKNOWLEDGEMENTS

We acknowledge support by the German Research Foundation through the Munich Center for Quantum Science and Technology (MCQST), Elite Network of Bavaria through the program ExQM, EU Flagship project QMiCS (Grant No. 820505), JST ERATO (Grant No. JPMJER1601).

## AUTHOR CONTRIBUTIONS

K.G.F. and F.D. planned the experiment. M.R., S.P., and K.G.F. performed the measurements and analyzed the data. M.R. and K.G.F. developed the theory. Q.C., Y.N., and M.P. contributed to development of the measurement software and experimental set-up. K.I. and Y.N. provided the JPA samples. F.D., A.M., and R.G. supervised the experimental part of this work. M.R. and K.G.F. wrote the manuscript. All authors contributed to discussions and proofreading of the manuscript.

## COMPETING INTERESTS

The authors declare no competing interests.

## ADDITIONAL INFORMATION

**Supplementary Information** The online version contains supplementary material available at https://doi.org/10.1038/s41534-021-00495-y.

**Correspondence** and requests for materials should be addressed to M. Renger or K. G. Fedorov.

**Reprints and permission information** is available at http://www.nature.com/reprints